Search for Magnetoelectric Coupling at the $^{57}Fe/Hf_{0.5}Zr_{0.5}O_2$ Interface Using Operando Synchrotron Mössbauer Spectroscopy

Vitaly Mikheev, Roberto Mantovan, Sergei Zarubin, Anna Dmitriyeva, Elena Suvorova, Philipp A. Buffat, and Andrei V. Zenkevich*

Multiferroic materials with coexisting ferroelectric and ferromagnetic orders have attracted much attention due to the magnetoelectric coupling opening alternative prospects for electronic devices. Composite multiferroics containing separate ferroelectric and ferromagnetic components are a promising alternative to the single-phase counterparts. Composite multiferroic structures comprising HfO_2-based ferroelectrics are potentially feasible for technological applications. Here, this study reports on the experiments aiming at the manifestation of magnetoelectric coupling at $Fe/Hf_{0.5}Zr_{0.5}O_2$ (HZO) interface. Using synchrotron based ^{57}Fe Mössbauer spectroscopy technique in operando, this study probes element-selectively the local magnetic properties of a nanometer-thick enriched ^{57}Fe marker layer in functional $Pt/^{57}Fe/HZO/TiN$ capacitors and demonstrates the evidence of the ferroelectric polarization effect on the α-Fe magnetic response. Besides α-Fe exhibiting a magnetoelectric coupling, both ferromagnetic and superparamagnetic Fe_3O_4 components are found in the Mössbauer spectra, apparently originating from the oxygen or OH^- ions penetrating ultrathin Pt overlayer during crystallization annealing of HZO. The observed effect as well as the electronic band lineup of the Fe/HZO interface elucidated from synchrotron based hard X-ray photoemission spectroscopy measurements are interpreted in terms of charge-mediated magnetoelectric coupling at the Fe/HfO_2 interface driven by ferroelectric HZO polarization reversal.

1. Introduction

Composite multiferroic materials exhibiting magnetoelectric (ME) coupling between ferromagnetic (FM) and ferroelectric (FE) orders are of great scientific interest and can be potentially used in multifunctional electronic device concepts.[1,2] Switching magnetization by applied electric rather than magnetic field or spin-polarized current requires much less energy,[3–5] making multiferroics promising for memory and logic applications.[6,7] Due to a limited number of single-phase multiferroic compounds operating at room temperature, composite multiferroics containing FM and FE components have been considered as viable candidates.[8–11] Composite multiferroic materials may have significant ME coupling comparable to their single-phase counterparts, which originates from strain-[12–15] or charge-mediated,[16–22] ion migration,[23] and even morphological changes[24,25] as coupling mechanisms.

Over the last decade, a wide range of materials[2] has been assessed as components in composite ME multiferroic materials ultimately aiming at technological applications. In particular, ME effects have been theoretically predicted and experimentally observed at the interface of the model FM and FE materials, such as $Fe/BaTiO_3$.[16,19] Within these efforts, however, the challenge is the compatibility with silicon-based technologies, and classical perovskite ferroelectrics have poor compatibility with the CMOS technology. Ferroelectricity discovered in doped or alloyed hafnia (HfO_2) films[26,27] has stimulated studies of their relevant properties.[28–34] It has been further demonstrated the applicability of

V. Mikheev, S. Zarubin, A. Dmitriyeva, A. V. Zenkevich
Moscow Institute of Physics and Technology
9, Institutskiy lane, Dolgoprudny, Moscow region 141701, Russia
E-mail: zenkevich.av@mipt.ru

R. Mantovan
CNR-IMM Unit of Agrate Brianza
Via Olivetti 2, Agrate Brianza, MB 20864, Italy

E. Suvorova
A.V. Shubnikov Institute of Crystallography
Federal Scientific Research Centre "Crystallography and Photonics"
Russian Academy of Sciences
Leninsky prospect, 59, Moscow 119333, Russia

P. A. Buffat
Ecole Polytechnique Fédérale de Lausanne
Centre Interdisciplinaire de Microscopie Electronique
Lausanne CH-1015, Switzerland

**ADVANCED
SCIENCE NEWS**

www.advancedsciencenews.com

**ADVANCED
MATERIALS
INTERFACES**

www.advmatinterfaces.de

ferroelectric hafnia to nonvolatile memory devices, such as FE random access memory (FeRAM),[35] FE field-effect transistors (FeFET),[36,37] and FE tunnel junctions FTJs.[38–40]

Furthermore, due to the excellent insulating properties, ferroelectricity persisting down to a nanometer thickness[41,42] and good compatibility with the Si-based semiconductor process,[36,37,41–43] doped hafnia thin films are expected to serve as a promising FE component in multiferroic heterostructures potentially feasible for technological applications. In this regard, exploring the ME effect at the ferroelectric/ferromagnetic interface in the heterostructures comprising doped HfO_2 as a FE constituent[44] is crucial for searching alternative composite multiferroics compatible with Si technology. In particular, strong charge-mediated ME coupling at the Ni/HfO_2 interface driven by FE HfO_2 polarization reversal has been predicted using density functional theory calculations.[45] Depending on the polarization orientation, a sizable difference in the interfacial Ni−O bonding as well as screening charges was found, which affected the relative population of the exchange-split majority- and minority-spin bands at the interface and eventually gave rise to significant changes of the interfacial magnetic moments. Recently, these predictions were confirmed by the experimental observation of the ME coupling effect at the interface between an ultrathin ferromagnetic Ni layer and an alloyed ferroelectric $Hf_{0.5}Zr_{0.5}O_2$ (HZO) thin film. Using the combination of operando synchrotron based spectroscopic techniques, clear evidence of the ferroelectric polarization effect on the magnetic response of a nanometer-thick Ni marker layer in functional Au/Co/Ni/HZO/W capacitors has been demonstrated.[46]

Mössbauer spectroscopy is a powerful technique capable of sensing tiny changes of magnetic properties at the atomic scale, and is especially useful when employed to analyze a few monolayers thick marker layers enriched with Mössbauer isotope placed at the interface.[47–50] In this work, we used synchrotron Mössbauer source (SMS)[51,52] at the European Synchrotron Radiation Facility to monitor in operando the effect of polarization reversal in ferroelectric $Hf_{0.5}Zr_{0.5}O_2$ (FE-HZO) on the magnetic properties of ≈1 nm thick Fe marker layer in Pt-^{57}Fe/FE-HZO/TiN based functional capacitor serving as "prototype memory devices." The choice of an ultrathin Fe layer 95% enriched in Mossbauer ^{57}Fe isotope as a magnetic counterpart in the prospective bilayer composite multiferroic is dictated by the possibility of performing unique experiments using the dedicated ^{57}Fe SMS. Polycrystalline thin-film alloyed HZO is the most popular HfO_2 based FE due to the relatively low crystallization temperature to form a metastable non-centrosymmetric phase, thus making it potentially compatible with the so-called back-end-of-line process in the electronic technology, while TiN underlayer is a standard electrode mainly used in HfO_2 based FE capacitors. In addition, a "sister" (Co/Fe)/FE-HZO/TiN sample was produced in order to further stabilize magnetic properties of the Fe layer in contact with ferroelectric HZO thus facilitating the use of the magnetic circular dichroism in angular distribution (MCDAD) technique complementary to the hard X-ray photoemission spectroscopy (HAXPES). The detailed description of the sample preparation procedure is given in the Experimental Section.

Following in situ polarization switching "up" or "down" in FE-HZO of the stripe-like Pt-^{57}Fe/FE-HZO/TiN capacitor device by a triangular voltage pulse −2 or +2.4 V (t = 100 μs) (the pulse amplitude optimized to avoid the risk of electric breakdown), we acquired two independent Mossbauer spectra for opposite polarization orientations. By accurately analyzing the obtained spectra, we observed statistically reliable changes in the line ratio of magnetically split α-^{57}Fe spectral component, pointing at the change of the Fe magnetic moment orientation, and thus manifesting room temperature ME coupling at Fe/FE-HZO interface. The data obtained in operando experiments are supplemented by high-resolution transmission electron microscopy and energy-dispersive X-ray analysis (HRTEM/EDX) of the sample cross section providing crucial insight into the structural properties and apparent intermixing in a bilayered Pt-^{57}Fe electrode during the sample preparation. In addition, hard X-ray photoemission spectroscopy (HAXPES) analysis was used to derive the electronic band alignment at the Fe/FE-HZO interface. The obtained results are explained in terms of the charge redistribution at the Fe/FE-HZO interface which affects the relative population of the majority- and minority-spin bands at the interface split by exchange interaction in ferromagnetic Fe and eventually gives rise to changes of the interfacial magnetic moment.[45] Small changes in the FeO_x/Fe area ratio observed in MS spectra following FE polarization reversal indicate a reversible redox reaction involving either the O atoms from HZO at the interface or alternatively the drift in/out of O^- and/or OH^- ions from the atmosphere through an ultrathin Pt layer in the electric field of HZO ferroelectric charges following the switching of polarization.[53]

2. Results and Discussion

The schematic of the operando synchrotron based Mossbauer spectroscopy experiment on the ferroelectric Pt-^{57}Fe/FE-HZO/TiN capacitors is shown in **Figure 1**a, while the sample on the holder and its exact geometric layout are shown in Figure S1a,b (Supporting Information), respectively. $P(V)$ curve displayed in Figure 1b for the stripe-like capacitor devices subjected to Mössbauer measurements are derived from the pulsed switching of polarization using PUND methodology (described in Section S2, Supporting Information). We note that while test Pt-^{57}Fe/FE-HZO/TiN capacitors 100 μm in diameter on the same chip exhibited $2P_r$ ≈ 36–40 μC cm^{-2} following ±3 V voltage sweep and standard initial electrical cycling ("wakeup") (Figures S2 and S3, Supporting Information), the remnant polarization value on the stripe-like capacitor devices is only $2P_r$ ≈ 10 μC cm^{-2}. Such discrepancy is explained by our experimental conditions, i.e., an unsaturated ferroelectric polarization switching expected for a limited voltage sweep (−2/+2.4 V) in order to avoid electrical breakdown of quite large (≈0.4 mm^2) capacitors required to fit the footprint of X-ray beam at the grazing incidence.

The experimental Mössbauer spectra (upon subtracting the background and parasitic contribution of Fe contamination in the Be lens optics at the beamline, Section S3, Supporting Information) of an ≈1 nm thick marker ^{57}Fe layer in contact with ferroelectric HZO in Pt/^{57}Fe/HZO/TiN capacitor devices acquired upon in situ switching the polarization in "down" and
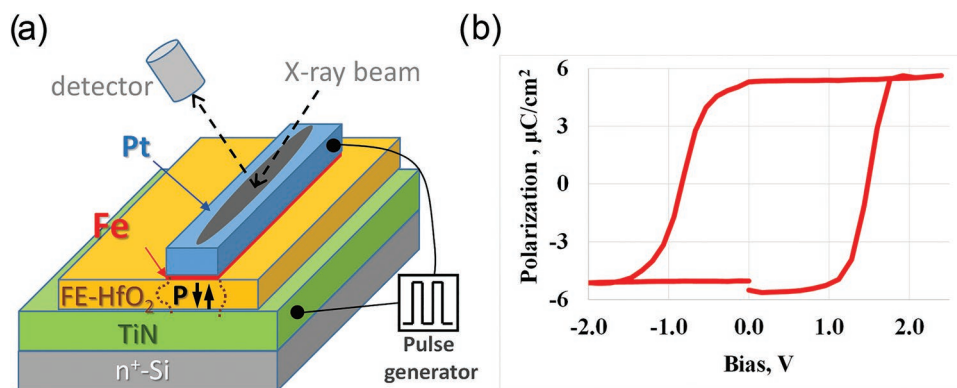
Figure 1. a) Schematic of the operando synchrotron based Mossbauer spectroscopy experiment on the ferroelectric Pt-^{57}Fe/FE-HZO/TiN capacitors; b) $P(V)$ curve taken in situ for the $50 \times 8000\ \mu m^2$ Pt-Fe^{57}/HZO/TiN ferroelectric capacitor device used in the experiments ($2P \approx 10\ \mu C\ cm^{-2}$).

"up" directions are displayed in **Figure 2** (left panel). Before revealing any effect of the ferroelectric polarization reversal in the Mössbauer spectra, one first needs to identify all the spectral components being associated with the chemical composition of the ^{57}Fe layer. The best fit of both experimental spectra is obtained by including four spectral components: three magnetic sextets and a paramagnetic doublet. The parameters of these spectral components are collected in the **Table 1**, where B_{hf} is hyperfine magnetic field at the ^{57}Fe nuclei, δ is isomer shift, ΔE_Q is quadrupole splitting, and "Δ area $P_{up} - P_{down}$" is the relative variation of the magnetic contributions area upon the switch of the HZO FE polarization.

The dominant magnetic contribution is due to the magnetically split α-Fe sextet (Table 1), while the hyperfine parameters identifying the other $Fe^{2.5+}$ and Fe^{3+} sextets (as indicated in Table 1) match those reported for the octahedral and tetrahedral sites of magnetite (Fe_3O_4), respectively.[60] The additional unresolved paramagnetic doublet in the center ("doublet" in Table 1 and corresponding green line in Figure 2) most likely

represents superparamagnetic Fe_3O_4 particles[61] (the bottom row in Table 1). The presence of Fe_3O_4 phase in the top layer is further corroborated by TEM analysis presented below. The most reasonable explanation for the partial Fe oxidation to Fe_3O_4 is the reaction with (atomic) oxygen by dissociating residual O_2 molecules in N_2 atmosphere on the surface of and penetrating through an ultrathin Pt (≈ 7 nm) overlayer during RTA aiming at the crystallization of HZO. The alternative explanation in terms of redox reaction at Fe/HZO interface will be considered below when analyzing photoemission spectra acquired by HAXPES.

We now focus on the analysis of the magnetically split sextet of α-Fe component in contact with HZO. The fitting of the experimental spectra reveals α-Fe lines' area ratio to be around $A_{16}{:}A_{25}{:}A_{34} \approx 3{:}3{:}1$ (Figure 2, left panel). Generally, the line ratio in a magnetically split Mössbauer sextet reflects the (averaged) magnetic moment direction in the Fe layer. In particular, the lines' intensity in Mössbauer spectra recorded in the synchrotron experiment here presented, is defined as[52]
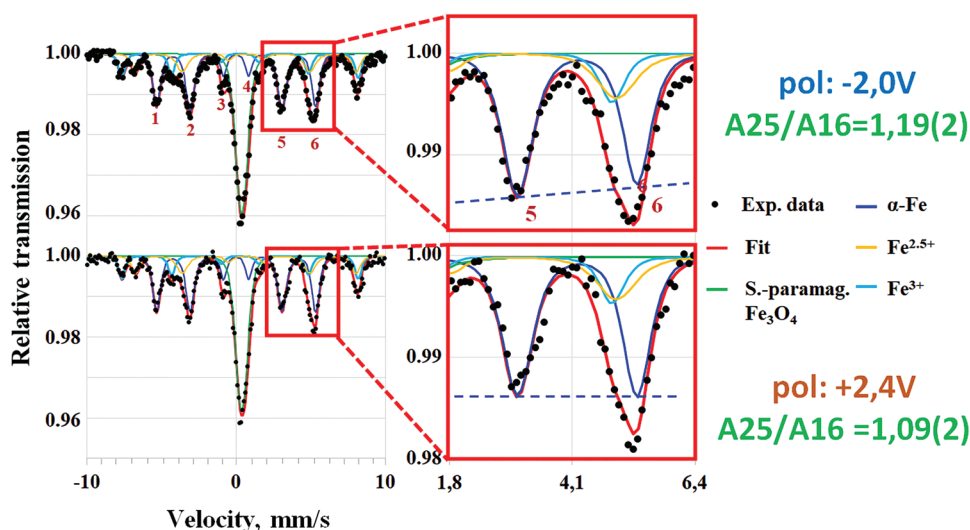
Figure 2. Experimental Mossbauer spectra taken from ^{57}Fe marker layer in Pt/^{57}Fe/HZO/TiN ferroelectric capacitor device for two opposite ferroelectric polarization orientations fitted with the model described in the text (left panel); the effect of polarization reversal on α-Fe lines' area ratio (right panel, α-Fe is represented by blue line).

ADVANCED
SCIENCE NEWS

www.advancedsciencenews.com

ADVANCED
MATERIALS
INTERFACES

www.advmatinterfaces.de

Table 1. Parameters of the spectral components in the Mössbauer spectrum taken from Pt-^{57}Fe/FE-HZO/TiN sample.

Component	Area [%]	B_{hf} [T]	δ [mm s^{-1}]	ΔE_Q [mm s^{-1}]	Δ area $P_{up} - P_{down}$ [%]
α-Fe	39.6	32.9	0	0	-1.5 ± 0.6
Fe$^{2.5+}$	14.3	45.7	0.66	0	0.9 ± 0.9
Fe^{3+}	12.5	49	0.27	0	0.6 ± 0.3
Doublet	33.6	–	0.38	0.36	–

$$I_{1,6} \propto 3 \cdot \sin^2(\alpha) \qquad (1)$$

$$I_{2,5} \propto 4 \cdot \cos^2(\alpha) \qquad (2)$$

$$I_{3,4} \propto 1 \cdot \sin^2(\alpha) \qquad (3)$$

where α is the angle between the vectors of the hyperfine magnetic field in the sample and the vector of magnetic field of SMS photons (directed horizontally, perpendicular to the beam direction, see Figure S5, Supporting Information). We note that in case of random distribution of magnetic moments with respect to the beam, the ratio would 3:4:1. The revealed line area ratio $A_{16}:A_{25}:A_{34} \approx 3{:}3{:}1$ suggests that the average $\alpha = arctg\sqrt{\frac{4}{3}} \cong 49°$.

Therefore, assuming that the sample magnetization vector lies in plane of the sample, it means that it is predominantly slightly oriented in the direction of the beam. (Note that the sample was not magnetized prior to SMS measurements.)

In order to reveal possible changes in the magnetization vector orientation following the ferroelectric polarization reversal, one has monitor for α-Fe the relative ratio A_{25}/A_{16} of lines 2 plus 5 area with respect to that of lines 1 plus 6. Indeed, in situ switching of ferroelectric polarization in HZO layer of the capacitor device results in the changes of the α-Fe line area ratio A_{25}/A_{16} is equal to 1.09 ± 0.02 and 1.19 ± 0.02 for P_{up} and P_{down}, respectively (Figure 2, right panel). We emphasize that the difference in the α-Fe line ratio for two opposite polarization orientations is beyond the experimental error and can therefore be taken as the evidence of the changes in the magnetic properties of α-Fe marker layer in contact with FE-HZO. As was pointed above, the line ratio in the magnetic line depends on the magnetic moment orientation with respect to the magnetic field vector in X-ray beam. Therefore, we take the observed difference of the α-Fe line ratio for opposite ferroelectric polarization orientations in the adjacent HZO layer as an evidence of the (room temperature) magnetoelectric coupling effect at the Fe/HZO interface.

In addition, we detect that the ferroelectric polarization reversal in HZO gives rise to the small, but measurable change in the relative area ratio between α-Fe and Fe$_3$O$_4$ lines (right column in Table 1), hinting that there might be an electric field induced redox reaction of Fe with the oxygen and/or the H$^+$/OH$^-$ ions either from the air penetrating a Pt overlayer or with the oxygen in HZO contacting Fe.

In order to get further insight into the origin of the observed effect of FE polarization reversal on the α-Fe lines' area ratio in the SMS experiment, we carefully explore the structural properties of the Pt-^{57}Fe/FE-HZO/TiN sample under investigation by
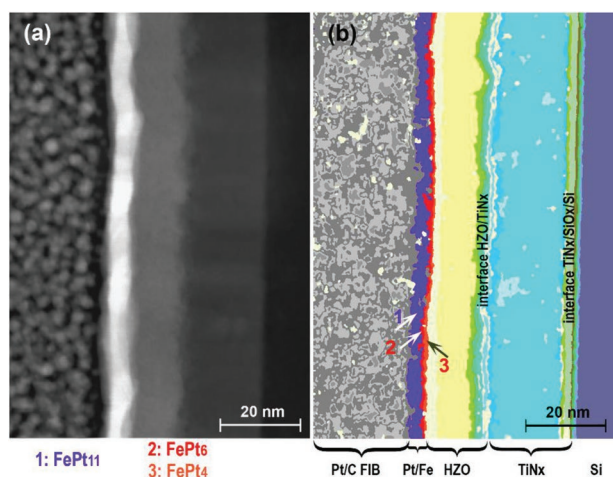
HRTEM analysis of the capacitor device cross section (**Figure 3**). By looking at the top metal layer it is impossible to clearly separate the individual Fe and Pt layers, suggesting that they are intermixed. The elemental mapping of as grown sample cross-section shows (see **Figure 4**) that although Pt and HZO ferro-electric phase), Fe is mostly present at the interface with HZO layer. EDX data also confirm the presence of oxygen in Pt-Fe top metal layer. In order to identify phase composition of the top metal layer, we performed crystallographic phase analysis at the nano level using fast Fourier transform (FFT) analysis of several selected areas of the Pt-Fe layer (one example marked by a square is shown in Figure 3,a). The analysis of FFT patterns confirmed the presence of Pt and Fe$_3$O$_4$ (nano)grains[56] present in Pt-Fe layer, in agreement with Mössbauer data. However, in FFT images taken from areas suitable for Fourier analysis we did not find α-Fe phase which is evident from the Mössbauer spectra. This result indicates that there are only separate α-Fe grains present at the interface with HZO rather than a continuous layer (unless metallic Fe is fully oxidized during preparation of the sample cross section).

The electronic band lineup at the Fe/HZO interface was reconstructed using standard HAXPES methodology[63,64] on a "sister" Co/Fe/HZO/W sample produced with the same methodology. By measuring the binding energies of the core-level Fe 2p (Figure S5a, Supporting Information), Hf4f line (**Figure 5**a) and taking the work function (WF) of Fe WF$_{Fe} \approx 4.65$ eV, the electron affinity of HfO$_2$ $\chi \approx 2$ eV and its bandgap $E_g \approx 5$ eV,[41] we get the conduction band offset (CBO) ≈ 1 eV (Figure 5), implying a very large electric dipole built up at the Fe/HZO interface with negative charges accumulated at the Fe side.

In addition, in situ polarization switching in Co/Fe/HZO/W ferroelectric capacitor during HAXPES experiment resulted in the change of the band offset ΔCBO ≈ 0.2 eV, indicating that ferroelectric charges contribute to the band lineup.[54]
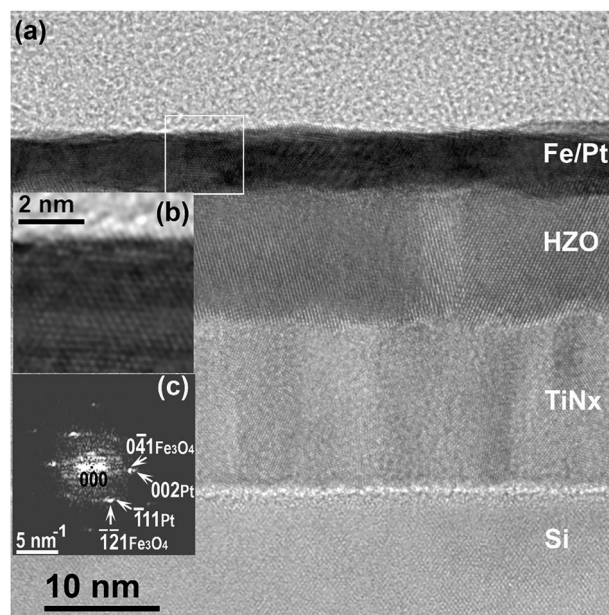
Figure 3. Cross section of sample: a) HRTEM image, b) HRTEM filtered image and c) FFT (c) obtained from the selected area 6.6 nm × 6.6 nm.

**ADVANCED
SCIENCE NEWS**

www.advancedsciencenews.com

**ADVANCED
MATERIALS
INTERFACES**

www.advmatinterfaces.de

**Figure 4.** Cross section: a) HAADF STEM image and b) the corresponding EDXS-phase map.

It was suggested recently (for Ni/HZO interface[46]) that the negative charges on the ferromagnetic metal side originate from the unbound electrons resulting from oxygen vacancies formed in HZO due to the redox reaction at the metal/HZO interface. These electrons change the relative population close to the Fermi level of the majority- and minority-spin bands split by exchange interaction in the interfacial ferromagnetic layer irrespective of ferroelectric polarization orientation. Furthermore, it was found[46] that the switching of the polarization orientation affects the interfacial Ni—O bonding as well as screening charges, the population of the majority- and minority-spin bands at the interface and eventually gives rise to significant changes of the interfacial magnetic moment. We believe that our current results related to the Fe/HZO interface can be explained in the framework of this theory. This suggests that the ME coupling provided by HZO could be a general mechanism being exploitable at the interface with 3d-ferromagnetic layers.

In our SMS experiment, depending on the ferroelectric polarization orientation we observe small, but statistically reliable change in the area ratio of α-Fe spectral components pointing at the change of the magnetic moment orientation with respect to the direction of the incident X-ray beam. In addition, we observe some changes in the α-Fe versus Fe_3O_4 spectral components areal ratio indicating the redox reaction at the Fe/HZO interface. The change in the electric dipole value depending on the polarization vector orientation revealed from HAXPES analysis is also consistent with the HZO redox reaction and Fe oxidation at the Fe/HZO interface.

It is worth noting that due to the intermixing of Pt and Fe sublayers and the partial oxidation of the latter only small part of Fe atoms are presumably affected by any charge-mediated magnetoelectric effect at the Fe/HZO interface. Once such detrimental intermixing effect is excluded and the ferromagnetism in a few monolayer thick α-Fe is stabilized by another magnetic layer, such as Co used in our "sister" sample (Figure S5b, Supporting Information), the effect observed in operando Mössbauer experiment should be expected much larger.

3. Conclusion

Composite multiferroics containing separate ferroelectric and ferromagnetic components often have much larger magnetoelectric coupling compared to their single-phase counterparts and can thus serve the functional basis of novel multifunctional electronic devices. Doped/alloyed ferroelectric HfO_2 thin films compatible with modern microelectronics may be a promising component in composite multiferroic structures potentially feasible for technological applications. In this work, we have used operando synchrotron Mössbauer spectroscopy technique to probe element-selectively the local magnetic properties of a nanometer-thick ^{57}Fe marker layer in functional $Pt/^{57}Fe/HZO/TiN$ capacitors. We have demonstrated that the reversal of ferroelectric polarization orientation in HZO gives rise to the change of magnetically spit line area ratio in α-Fe component,
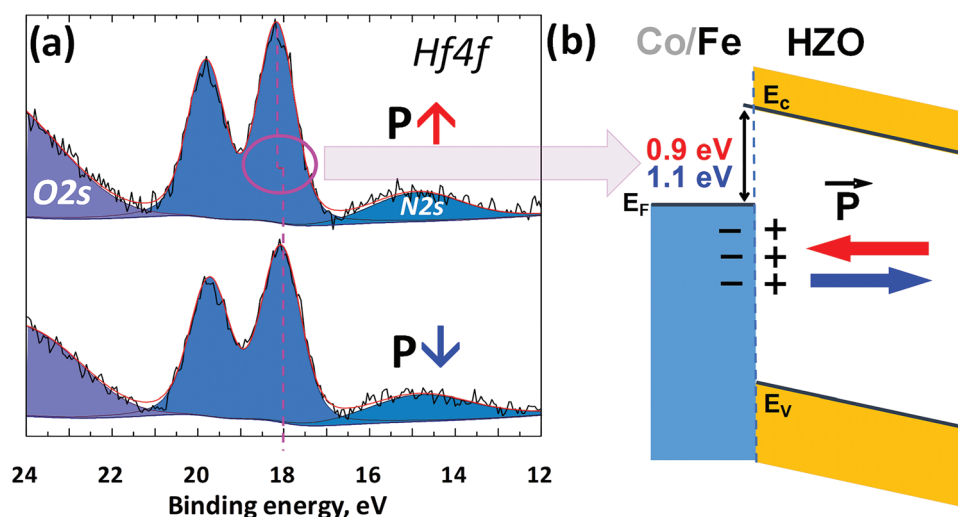
Figure 5. a) Hf4f core-level spectra taken at two opposite ferroelectric orientations in HZO with the top (Co)Fe electrode grounded; b) the effect of polarization reversal on the electronic band lineup at the Fe/HZO interface.

2201341 (5 of 8)

**ADVANCED
SCIENCE NEWS**

www.advancedsciencenews.com

**ADVANCED
MATERIALS
INTERFACES**

www.advmatinterfaces.de

which manifests a room temperature magnetoelectric coupling effect at the Fe/HZO interface. Both ferromagnetic and superparamagnetic Fe_3O_4 components also found in the Mössbauer spectra originate from the atomic oxygen or OH^- ions penetrating ultrathin Pt overlayer during the crystallization annealing of HZO. The observed effect of HZO polarization orientation on the magnetic properties of an Fe marker layer as well as on the electronic band lineup at the Fe/HZO interface elucidated by HAXPES are interpreted in terms of charge-mediated magnetoelectric coupling at the Fe/HfO_2 interface driven by ferroelectric HZO polarization reversal. In addition, small, but statistically reliable changes of Fe_3O_4/α-Fe area ratio in Mössbauer spectra following the polarization switching indicate (reversible) redox reaction attributed to the presence of O and/or OH^- ions at the interface, which is induced by ferroelectric charges of opposite signs.

4. Experimental Section

The samples were grown on the pre-oxidized Si chips 1.5×1.5 cm^2 in size. First, the 50 nm-thick TiN layer was deposited by magnetron sputtering. $Hf_{0.5}Zr_{0.5}O_2$ (HZO) layer 10 nm in thickness was grown by atomic layer deposition (ALD) on top. The HZO growth process was described in detail previously.[41,54] 1-nm-thick Fe marker layer enriched in ^{57}Fe isotope to 95% and the capping 7-nm-thick Pt overlayer were both deposited by pulsed laser deposition in ultrahigh vacuum in a single vacuum cycle on HZO with thicknesses carefully optimized to ensure continuous film coverage, sufficient conductivity, and reasonably high yield of X-rays exhibiting nuclear resonant scattering. In order to stabilize the non-centrosymmetric orthorhombic phase, the as-grown structures were exposed to rapid thermal annealing (RTA) at $T = 400$ °C, 30 s in N_2 atmosphere. The obtained tri-layer heterostructure was patterned into functional ferroelectric capacitor devices with lateral dimensions 50×8000 µm^2 chosen to match the grazing incidence X-ray beam footprint at the beamline ID18 of the European Synchrotron Radiation Facility (ESRF). To ensure the ability of in situ pulsed switching and polarization measurements from the remote source-meter unit the metal pads ≈ 0.25 mm^2 in size connected to capacitor electrodes were also fabricated on the chip. Some details are provided in Section S1 (Figure S1, Supporting Information).

The ferroelectric properties of the fabricated $Pt/^{57}Fe/HZO/TiN$ capacitors were examined ex situ by using Cascade Summit 1100 probe station coupled with Agilent semiconductor device analyzer B1500A and in situ during SMS analysis with Agilent B2912A source-measure unit. In both cases, pulsed switching and the positive-up negative-down (PUND) technique[46] were implemented (for details see Section S2, Supporting Information).

Operando SMS experiments were performed at the nuclear resonance beamline (ID18)[60] of ESRF. SMS was operated using (111) reflection of $^{57}FeBO_3$ crystal with source linewidth of 0.25 mm s^{-1} and intensity of about 2×10^4 photons s^{-1}. More details about the instrument can be found in ref. [51]. Beam from SMS was focused using Kirkpatrick–Baez mirror to the spot size of 22 µm × 14 µm (vertical × horizontal, FWHM). Mössbauer spectra were measured at the incidence angle of 0.17°, i.e., well above the critical angle of HfO_2 (about 0.22°). Under these conditions, the measured spectra can be and were treated as conventional Mössbauer absorption spectra. All SMS measurements were performed at room temperature. The fitting of the acquired Mössbauer spectra was carried out with the Vinda software package.[56]

HAXPES measurements were performed at the beamline P22 of PETRA III (DESY) with Specs 225 HV analyzer, choosing an excitation energy $E = 6$ keV with an overall energy resolution of about 0.2 eV.[57] The spectra were acquired on a "sister" Co/Fe/HZO/W sample. In order to optimize the photoelectron flux and the probing depth the sample was placed in the grazing X-ray incidence angle. To reconstruct electronic band alignment at the Fe/HZO interface and its evolution upon polarization reversal, the Hf4f and Fe2p core-level spectra were acquired in short-circuit configuration, with both electrodes kept grounded. The direction of polarization was controlled in situ with help of Agilent B2912A source-measure unit, plugged to the sample in the measuring chamber. In addition, core-level spectra of bulk pure Fe and HZO sample were taken as a reference. Spectra analysis was performed in Unifit 2015 software suite.[58]

Thin cross sections of one of capacitor devices under investigation were prepared with the focused ion beam technique at room temperature using the JIB-4501 MultiBeam SEM-FIB System (JEOL, Japan). HRTEM and scanning TEM (STEM) images, and energy-dispersive X-ray spectrometry (EDXS) microanalysis were obtained at the accelerating voltage $E = 200$ kV on an analytical field emission transmission electron microscope (FEI Tecnai Osiris) fitted with a 4 SDD detectors Super X ChemiSTEM EDXS system running under ESPRIT software (Bruker). The principal component analysis (PCA) method was used to extract from the spectrum-image data cube statistical groups that can be interpreted as phases. A phase image using the clusters method was created based on the chemical information stored in every pixel of an acquired map. Colored EDXS maps that reveal the local distribution of different phases in a sample, with particular interest being paid to the detection of the Pt/Fe/O component were produced. Crystallographic phase analysis was performed using the HRTEM Fourier Transform diffractograms (FFT) which were processed with the DigitalMicrograph suite GMS 2.31 (Gatan Inc.) and interpreted with the JEMS software.[59]

Supporting Information

Supporting Information is available from the Wiley Online Library or from the author.

Conflict of Interest

The authors declare no conflict of interest.

Data Availability Statement

The data that support the findings of this study are available from the corresponding author upon reasonable request.

[1] W. Eerenstein, N. Mathur, J. F. Scott, *Nature* **2006**, *442*, 759.

[2] N. A. Spaldin, R. Ramesh, *Nat. Mater.* **2019**, *18*, 203.

[3] E. Y. Tsymbal, *Nat. Mater.* **2012**, *11*, 12.

[4] S. Manipatruni, D. E. Nikonov, I. A. Young, *Nat. Phys.* **2018**, *14*, 338.

[5] P. B. Meisenheimer, S. Novakov, N. M. Vu, J. T. Heron, *J. Appl. Phys.* **2018**, *123*, 240901.

[6] J. F. Scott, *Nat. Mater.* **2007**, *6*, 256.

[7] M. Bibes, A. Barthélémy, *Nat. Mater.* **2008**, *7*, 425.

[8] L. W. Martin, S. P. Crane, Y.-H. Chu, M. B. Holcomb, M. Gajek, M. Huijben, C.-H. Yang, N. Balke, R. Ramesh, *J. Phys.: Condens. Matter* **2008**, *20*, 434220.

[9] J. P. Velev, S. S. Jaswal, E. Y. Tsymbal, *Philos. Trans. R. Soc.* **2011**, *A369*, 3069.

[10] C. A. F. Vaz, *J. Phys.: Condens. Matter* **2012**, *24*, 333201.

[11] J.-M. Hu, C.-G. Duan, C.-W. Nan, L.-Q. Chen, *npj Comput. Mater.* **2017**, *3*, 18.

[12] C.-W. Nan, M. I. Bichurin, S. Dong, D. Viehland, G. Srinivasan, *J. Appl. Phys.* **2008**, *103*, 031101.

[13] T. X. Nan, Z. Y. Zhou, J. Lou, M. Liu, X. Yang, Y. Gao, S. Rand, N. X. Sun, *Appl. Phys. Lett.* **2012**, *100*, 132409.

[14] K. J. A. Franke, D. López González, S. J. Hämäläinen, S. van Dijken, *Phys. Rev. Lett.* **2014**, *112*, 017201.

[15] Q. Wang, X. Li, C.-Y. Liang, A. Barra, J. Domann, C. Lynch, A. Sepulveda, G. Carman, *Appl. Phys. Lett.* **2017**, *110*, 102903.

[16] C. G. Duan, S. S. Jaswal, E. Y. Tsymbal, *Phys. Rev. Lett.* **2006**, *97*, 047201.

[17] K. Yamauchi, B. Sanyal, S. Picozzi, *Appl. Phys. Lett.* **2007**, *91*, 062506.

[18] H. J. A. Molegraaf, J. Hoffman, C. A. F. Vaz, S. Gariglio, D. van der Marel, C. H. Ahn, J.-M. Triscone, *Adv. Mater.* **2009**, *21*, 3470.

[19] G. Radaelli, D. Petti, E. Plekhanov, I. Fina, P. Torelli, B. R. Salles, M. Cantoni, C. Rinaldi, D. Gutiérrez, G. Panaccione, M. Varela, S. Picozzi, J. Fontcuberta, R. Bertacco, *Nat. Commun.* **2014**, *5*, 3404.

[20] Z. Zhou, B. M. Howe, M. Liu, T. Nan, X. Chen, K. Mahalingam, N. X. Sun, G. J. Brown, *Sci. Rep.* **2015**, *5*, 7740.

[21] A. Rajapitamahuni, L. L. Tao, Y. Hao, J. Song, X. Xu, E. Y. Tsymbal, X. Hong, *Phys. Rev. Mater.* **2019**, *3*, 021401.

[22] F. Motti, G. Vinai, A. Petrov, B. A. Davidson, B. Gobaut, A. Filippetti, G. Rossi, G. Panaccione, P. Torelli, *Phys. Rev. B* **2018**, *97*, 094423.

[23] X. Chen, X. Zhu, W. Xiao, G. Liu, Y. P. Feng, J. Ding, R.-W. Li, *ACS Nano* **2015**, *9*, 4210.

[24] G. Vinai, F. Motti, V. Bonanni, A. U. Petrov, S. Benedetti, C. Rinaldi, M. Stella, D. Cassese, S. Prato, M. Cantoni, G. Rossi, G. Panaccione, P. Torelli, *Adv. Electron. Mater.* **2019**, *5*, 1900150.

[25] F. Motti, G. Vinai, V. Bonanni, V. Polewczyk, P. Mantegazza, T. Forrest, F. Maccherozzi, S. Benedetti, C. Rinaldi, M. Cantoni, D. Cassese, S. Prato, S. S. Dhesi, G. Rossi, G. Panaccione, P. Torelli, *Phys. Rev. Mater.* **2020**, *4*, 114418.

[26] T. S. Böscke, J. Müller, D. Bräuhaus, U. Schröder, U. Böttger, *Appl. Phys. Lett.* **2011**, *99*, 102903.

[27] J. Müller, T. S. Böscke, U. Schröder, S. Mueller, D. Bräuhaus, U. Böttger, L. Frey, T. Mikolajick, *Nano Lett.* **2012**, *12*, 4318.

[28] D. Zhou, J. Müller, J. Xu, S. Knebel, D. Brauhaus, U. Schröder, *Appl. Phys. Lett.* **2012**, *100*, 082905.

[29] S. Clima, D. J. Wouters, C. Adelmann, T. Schenk, U. Schröder, M. Jurczak, G. Pourtois, *Appl. Phys. Lett.* **2014**, *104*, 092906.

[30] D. Martin, J. Müller, T. Schenk, T. M. Arruda, A. Kumar, E. Strelcov, E. Yurchuk, S. Müller, D. Pohl, U. Schröder, *Adv. Mater.* **2014**, *26*, 8198.

[31] S. Zarubin, E. Suvorova, M. Spiridonov, D. Negrov, A. Chernikova, A. Markeev, A. Zenkevich, *Appl. Phys. Lett.* **2016**, *109*, 192903.

[32] L. L. Tao, T. R. Paudel, A. A. Kovalev, E. Y. Tsymbal, *Phys. Rev. B* **2017**, *95*, 245141.

[33] Y.u. Matveyev, V. Mikheev, D. Negrov, S. Zarubin, A. Kumar, E. D. Grimley, J. M. LeBeau, A. Gloskovskii, E. Y. Tsymbal, A. Zenkevich, *Nanoscale* **2019**, *11*, 19814.

[34] Y. Wei, P. Nukala, M. Salverda, S. Matzen, H. J. Zhao, J. Momand, A. S. Everhardt, G. Agnus, G. R. Blake, P. Lecoeur, B. J. Kooi, J. Íñiguez, B. Dkhil, B. Noheda, *Nat. Mater.* **2018**, *17*, 1095.

[35] T. Francois, L. Grenouillet, J. Coignus, P. Blaise, C. Carabasse, N. Vaxelaire, T. Magis, F. Aussenac, V. Loup, C. Pellissier, *IEEE IEDM* **2019**, 15.7.1.

[36] S. Mueller, J. Müller, R. Hoffmann, E. Yurchuk, T. Schlösser, R. Boschke, J. Paul, M. Goldbach, T. Herrmann, A. Zaka, U. Schröder, T. Mikolajick, *IEEE Trans. Electron Dev.* **2013**, *60*, 4199.

[37] M. Seo, M.-H. Kang, S.-B. Jeon, H. Bae, J. Hur, B. C. Jang, S. Yun, S. Cho, W.-K. Kim, M.-S. Kim, K.-M. Hwang, S. Hong, S.-Y. Choi, Y.-K. Choi, *IEEE Electron Device Lett.* **2018**, *39*, 1445.

[38] F. Ambriz-Vargas, G. Kolhatkar, M. Broyer, A. HadjYoussef, R. Nouar, A. Sarkissian, R. Thomas, C. GomezYáñez, M. A. Gauthier, A. Ruediger, *ACS Appl. Mater. Interfaces* **2017**, *9*, 13262.

[39] A. Chouprik, A. Chernikova, A. Markeev, V. Mikheev, D. Negrov, M. Spiridonov, S. Zarubin, A. Zenkevich, *Microelectron. Eng.* **2017**, *178*, 250.

[40] Y. Goh, S. Jeon, *Appl. Phys. Lett.* **2018**, *113*, 052905.

[41] A. Chernikova, M. Kozodaev, A. Markeev, D. Negrov, M. Spiridonov, S. Zarubin, O. Bak, P. Buragohain, H. Lu, E. Suvorova, A. Gruverman, A. Zenkevich, *ACS Appl. Mater. Interfaces* **2016**, *8*, 7232.

[42] S. S. Cheema, D. Kwon, N. Shanker, R. dos Reis, S.-L. Hsu, J. Xiao, H. Zhang, R. Wagner, A. Datar, M. R. McCarter, C. R. Serraoe, *Nature* **2020**, *580*, 478.

[43] V. Mikheev, A. Chouprik, Yu. Lebedinskii, S. Zarubin, Yu. Matveyev, E. Kondratyuk, M. Kozodaev, A. Markeev, A. Zenkevich, D. Negrov, *ACS Appl. Mater. Interfaces* **2019**, *11*, 32108.

[44] Y. Wei, S. Matzen, C. P. Quinteros, T. Maroutian, G. Agnus, P. Lecoeur, B. Noheda, *npj Quantum Mater.* **2019**, *4*, 62.

[45] Q. Yang, L. Tao, Z. Jiang, Y. Zhou, E. Y. Tsymbal, V. Alexandrov, *Phys. Rev. Appl.* **2019**, *12*, 024044.

[46] A. Dmitriyeva, V. Mikheev, S. Zarubin, A. Chouprik, G. Vinai, V. Polewczyk, P. Torelli, Yu. Matveyev, C. Schlueter, I. Karateev, Q. Yang, Z. Chen, L. Tao, E. Y. Tsymbal, A. Zenkevich, *ACS Nano* **2021**, *15*, 14891.

[47] M. Fanciulli, A. Zenkevich, G. Weyer, *Appl. Surf. Sci.* **1998**, *123*, 207.

[48] R. Mantovan, C. Wiemer, A. Lamperti, M. Georgieva, M. Fanciulli, A. Goikhman, N. Barantsev, Yu. Lebedinskii, A. Zenkevich, *Hyperfine Interact.* **2009**, *191*, 41.

[49] A. Zenkevich, R. Mantovan, M. Fanciulli, M. Minnekaev, Yu. A. Matveyev, Yu. Lebedinskii, S. Thiess, W. Drube, *Appl. Phys. Lett.* **2011**, *99*, 182905.

[50] A. Cini, M. Mannini, F. Totti, M. Fittipaldi, G. Spina, A. Chumakov, R. Rüffer, A. Cornia, R. Sessoli, *Nat. Commun.* **2018**, *9*, 480.

[51] V. Potapkin, A. I. Chumakov, G. V. Smirnov, J.-P. Celse, R. Rüffer, C. McCammon, L. Dubrovinsky, *J. Synchrotron Radiat.* **2012**, *19*, 559.

[52] G. V. Smirnov, U. van Burck, A. I. Chumakov, A. Q. R. Baron, R. Ruffer, *Phys. Rev. B* **1997**, *55*, 5811.

[53] A. J. Tan, M. Huang, C. O. Avci, F. Büttner, M. Mann, W. Hu, C. Mazzoli, S. Wilkins, H. L. Tuller, G. S. D. Beach, *Nat. Mater.* **2019**, *18*, 35.

[54] R. Mantovan, S. Vangelista, S. Cocco, A. Lamperti, O. Salicio, *J. Appl. Phys.* **2011**, *111*, 078107.

[55] C. E. Johnson, J. A. Johnson, H. Y. Hah, M. Cole, S. Gray, V. Kolesnichenko, P. Kucheryavy, G. Goloverda, *Hyperfine Interact.* **2016**, *237*, 27.

[56] Y. Fei, D. J. Frost, H. O.-K. Mao, C. T. Prewitt, D. Hausermann, *Am. Mineral.* **1999**, *84*, 203.

[57] E. Kraut, R. Grant, J. Waldrop, S. Kowalczyk, *Phys. Rev. B* **1983**, *28*, 1965.

2201341 (7 of 8)

[58] Y. Lebedinskii, A. Zenkevich, E. Gusev, *J. Appl. Phys.* **2007**, *101*, 074504.

[59] Y. Matveyev, D. Negrov, A. Chernikova, Y. Lebedinskii, R. Kirtaev, S. Zarubin, E. Suvorova, A. Gloskovskii, A. Zenkevich, *ACS Appl. Mater. Interfaces* **2017**, *9*, 43370.

[60] R. Ruffer, A. I. Chumakov, *Hyperfine Interact.* **1996**, *97*, 589.

[61] H. P. Gunnlaugsson, *Hyperfine Interact.* **2016**, *237*, 79.

[62] C. Schlueter, A. Gloskovskii, K. Ederer, I. Schostak, S. Piec, I. Sarkar, Y. Matveyev, P. Lömker, M. Sing, R. Claessen, C. Wiemann, C. M. Schneider, K. Medjanik, G. Schönhense, P. Amann, A. Nilsson, W. Drube, *AIP Conf. Proc.* **2019**, *2054*, 040010.

[63] https://www.unifit-software.de/ (accessed: October 2022).

[64] P. Stadelmann, *JEMS* **2021**, https://www.jems-swiss.ch/ (accessed: October 2022).

2201341 (8 of 8)